Available online at www.sciencedirect.com
SCIENCE DIRECT
Journal of Catalysis 237 (2006) 162–174
JOURNAL OF CATALYSIS
www.elsevier.com/locate/jcat

Ni–Nb–O mixed oxides as highly active and selective catalysts for ethene production via ethane oxidative dehydrogenation. Part I: Characterization and catalytic performance

E. Heracleous, A.A. Lemonidou *

Department of Chemical Engineering, Aristotle University of Thessaloniki and Chemical Process Engineering Research Institute (CERTH/CPERI), PO Box 1517, University Campus, GR-54006 Thessaloniki, Greece

Received 21 September 2005; revised 2 November 2005; accepted 3 November 2005

Abstract

This work demonstrates the high potential of a new class of catalytic materials based on nickel for the oxidative dehydrogenation of ethane to ethylene. The developed bulk Ni–Nb–O mixed oxides exhibit high activity in ethane ODH and very high selectivity (∼90% ethene selectivity) at low reaction temperature, resulting in an overall ethene yield of 46% at 400 °C. Varying the Nb/Ni atomic ratio led to an optimum catalytic performance for catalysts with Nb/Ni ratio in the range 0.11–0.18. Detailed characterization of the materials with several techniques (XRD, SEM, TPR, TPD-NH_3, TPD-O_2, Raman, XPS, electrical conductivity) showed that the key component for the excellent catalytic behavior is the Ni–Nb solid solution formed upon the introduction of niobium in NiO, evidenced by the contraction of the NiO lattice constant, since even small amounts of Nb effectively converted NiO from a total oxidation catalyst (80% selectivity to CO_2) to a very efficient ethane ODH material. An upper maximum dissolution of Nb^{5+} cations in the NiO lattice was attained for Nb/Ni ratios $\leqslant$0.18, with higher Nb contents leading to inhomogeneity and segregation of the NiO and Nb_2O_5 phases. A correlation between the specific surface activity of the catalysts and the surface exposed nickel content led to the conclusion that nickel sites constitute the active centers for the alkane activation, with niobium affecting mainly the selectivity to the olefin. The incorporation of Nb in the NiO lattice by either substitution of nickel atoms and/or filling of the cationic vacancies in the defective nonstoichiometric NiO surface led to a reduction of the materials nonstoichiometry, as indicated by TPD-O_2 and electrical conductivity measurements, and, consequently, of the electrophilic oxygen species (O^-), which are abundant on NiO and are responsible for the total oxidation of ethane to carbon dioxide.

Keywords: Ethane; Oxidative dehydrogenation; Nickel oxide; Mixed nickel-niobium oxides; Nonstoichiometric oxygen

1. Introduction

Light olefins are currently produced by steam cracking of various petroleum fractions, mainly naphtha. The reactions that take place in a steam cracker are highly endothermic, and thus the process energy demands are extremely high. With the olefin market growing at a rate of 3% per year and fuel costs rising constantly, the development of a substitute method for the production of light olefins has become an increasingly urgent task.

The most attractive alternative to steam cracking is the catalytic dehydrogenation of light alkanes in the presence of an oxidizing agent [1]. The energy requirements are minimal because of the low operation temperature and mild exothermicity of the reaction, while alkanes constitute a low-cost and readily available feedstock, conforming to the general need for sustainable development. However, the development of both active and selective catalytic materials proves to be a very hard task, since the formation of carbon oxides is the thermodynamically favored route and the resulting product, alkene, is generally more reactive than the alkane. Therefore, a catalyst should be able to activate and selectively convert the alkane to the corresponding alkene at relatively low temperature and also preserve the alkene from secondary oxidation.

* Corresponding author.
E-mail address: alemonidou@cheng.auth.gr (A.A. Lemonidou).

0021-9517/$ – see front matter
doi:10.1016/j.jcat.2005.11.002

Ethane oxidative dehydrogenation has been studied over a wide range of catalytic materials. Supported early-transition metal oxides (V, Mo, Cr) operate at low temperature (<550 °C) and exhibit high initial ethene selectivity [2–6]. However, high activity can only be achieved at the expense of ethene production, because these catalysts are as a rule more reactive toward olefins. High ethylene yields have been reported over chlorine-promoted nonreducible oxides (e.g., LiCl/MgO), where the reaction proceeds at high temperature (>600 °C) via a homogeneous–heterogeneous reaction scheme [7–10]. Nonetheless, serious problems, such as low catalyst stability and the release of chlorine, are associated with the use of these catalysts.

Multicomponent mixed oxides seem to be the most promising class of materials for the ethane oxidative dehydrogenation reaction. One of the best-performing catalysts, reported in 1978 by Thorsteinson et al. [11], consists of a mixture of Mo–V–Nb oxides operating at low temperature (<400 °C) with relatively high efficiency. More recently, Lopez Nieto and co-workers have developed a catalytic formulation based on mixed Mo–V–Te–Nb oxides exhibiting about 75% ethylene yield at low reaction temperature (350–400 °C). The enhanced catalytic activity of the proposed mixed oxides was related to the presence of a multifunctional $Te_2M_{20}O_{57}$ (M = Mo, V, Nb) orthorhombic phase [12].

In a recent investigation we showed that nickel-based materials exhibit very good potential as catalysts for ethylene production via ethane oxidative dehydrogenation [13]. The good performance of nickel catalysts has been reported previously [14–18], but with no extensive characterization and/or identification of active sites. In our earlier study we demonstrated that spreading of NiO on alumina causes chemical modification of the NiO particles, which, even though possess a bulk-like crystallography, exhibit modified electronic properties (monitored by X-ray photoelectron spectroscopy [XPS]), rendering them active and selective in ethane ODH; in contrast, unsupported pure NiO was very unselective toward ethane [13]. Promotion of the NiO/Al_2O_3 catalysts with various metals (Mo, V, Co, Nb, and Ta) significantly modified both structural and catalytic properties. The introduction of niobium was the most beneficial for ethane ODH, increasing the reactivity toward ethane by >50% while maintaining the high ethene selectivity, resulting in a 30% ethene yield at 425 °C. Niobium was found to improve the dispersion of the nickel phase and facilitate the C–H bond activation by acting as an electron transfer promoter.

In the case of unpromoted NiO/Al_2O_3 catalysts, the presence of the alumina support was essential for achieving high selectivity in the ethane ODH reaction [13]. However, further investigation of the Nb-promoted catalyst revealed that supporting the nickel–niobium phase was not necessary and that actually the unsupported Ni–Nb–O mixed oxide yielded a much-improved catalytic material. We therefore report in this study the development of highly active and selective Ni–Nb–O mixed-oxide catalysts for the ethane oxidative dehydrogenation reaction. The effect of the Nb/Ni ratio on the performance of the materials is discussed in view of a detailed investigation of the bulk and surface properties of the oxides. Correlations between the characterization results and the catalytic performance data shed light on the nature and functionality of the catalytic active sites.

2. Experimental

2.1. Catalyst preparation

A series of mixed Ni–Nb–O oxides with varying Nb/Ni atomic ratio ranging from 0 to 0.67 was prepared by the evaporation method. Aqueous solutions containing the precursor salts, nickel nitrate hexahydrate (>99%, Merck) and ammonium niobium oxalate (99.99%, Aldrich), in appropriate amounts were heated at 70 °C under continuous stirring for 1 h to ensure complete dissolution and good mixing of the starting compounds. The solvent was then removed by evaporation under reduced pressure, and the resulting solids were dried overnight at 120 °C and calcined in synthetic air at 450 °C for 5 h. Pure NiO and Nb_2O_5 used as reference compounds were obtained from the decomposition of the corresponding precursors at 450 °C for NiO and 550 °C for Nb_2O_5 for 5 h in synthetic air.

The catalysts are referred to as Ni_xNb_y, where x and y indicate the atomic content of Ni and Nb, respectively, relative to the total metal content of the materials.

2.2. Catalyst characterization

Surface areas of the samples were determined by N_2 adsorption at 77 K, using the multipoint BET analysis method, with an Autosorb-1 Quantachrome flow apparatus. Prior to the measurements, the samples were dehydrated in vacuum at 250 °C overnight.

X-Ray diffraction (XRD) patterns were obtained using a Siemens D500 diffractometer, with Cu-K_α radiation. The morphology of the synthesized materials was examined by scanning electron microscopy (SEM) on a JEOL 6300 microscope, coupled with energy-dispersive X-ray analysis (EDX; Oxford Link ISIS-2000) for local elemental composition determination.

The reduction characteristics of the catalysts were studied by temperature-programmed reduction (TPR) experiments performed in a gas flow system equipped with a quadrupole mass analyzer (Omnistar, Balzers). Typically, the catalyst sample (50 mg) was placed in a U-shaped quartz reactor and pretreated in flowing He for 0.5 h at 450 °C, followed by cooling at room temperature. The temperature was then raised from room temperature to 800 °C at a rate of 10 °C/min in a 5% H_2/He flow (50 cm^3/min). The main (m/z) fragments registered were $H_2 = 2$, $H_2O = 18$, and $He = 4$.

NH_3 temperature-programmed desorption (TPD) was used to determine the acid properties. The experiments were conducted on the same apparatus as the TPR experiments described above. The catalysts (100 mg) were pretreated at 450 °C for 0.5 h and then cooled to 100 °C under He flow. The pretreated samples were saturated with 5% NH_3/He for 1 h at 100 °C, with subsequent flushing with helium at 100 °C for 1 h to remove the physisorbed ammonia. TPD analysis was carried out from 100 to 700 °C at a heating rate of 10 °C/min. The following (m/z)

fragments were registered: $NH_3 = 15$, $H_2O = 18$; $N_2 = 28$, $NO = 30$, $N_2O = 44$, and $NO_2 = 46$. Quantitative analysis of the desorbed ammonia was based on (m/z) 15.

The oxygen desorption properties of selected catalysts were studied by O_2-TPD measurements. The catalyst sample (200 mg) was pretreated in a flow of pure oxygen at 450 °C for 1 h and cooled to room temperature under the oxygen flow. The system was subsequently flushed with helium for 1 h, and the temperature was raised to 850 °C at a rate of 15 °C/min in He (50 cm^3/min). The reactor exit was monitored on-line by a quadrupole mass analyzer (Omnistar, Balzers), and the desorbed oxygen was detected by following the 32 (m/z) fragment.

Raman spectra were recorded at ambient temperature with a 785-nm diode laser excitation (laser power level, 200 mW) on a Renishaw Raman Spectrometer (type 1000) equipped with a CCD detector. The catalysts were pressed into self-supporting wafers and placed in a sample holder, consisting of a gold plate attached to a heating wire. Before the measurements, the samples were pretreated in flowing He at 120 °C for 1 h. The wavenumber accuracy was within 1 cm^{-1}.

The surface composition of the catalysts was determined by XPS. The XPS measurements were performed on a Kratos AXIS HSi instrument equipped with a charge neutralizer and Mg-K_α X-ray source. Spectra were recorded at normal emission, using an analyzer pass energy of 20 eV and X-ray power of 225 W.

Electrical conductivity measurements were performed on an Agilent 4284 A 20-kHz–1-MHz precision LCR meter. The samples were compressed under mild pressure to form pellets of approximately 10 mm diameter and 5 mm thickness, which were then coated with silver paste, as an electrode, on both surface sides. The electrical resistance (R) of the catalysts was measured at room temperature in atmospheric air in a frequency range of 100 kHz–1 MHz. The electrical conductivity (σ) was then computed using the formula $\sigma = R^{-1}tS^{-1}$, where t is the thickness and S the cross-sectional area of the pellet. The DC conductivity was calculated by fitting the AC conductivity dispersion with frequency using Jonscher's power law (JPL) [19], $\sigma_{AC} = \sigma_{DC} + A\omega^s$, by nonlinear least squares fit analysis, where A is a constant and s is a power law exponent.

2.3. Reactivity studies

The catalytic performance of the samples was measured in a fixed-bed quartz reactor. The catalyst particles were diluted with equal amount of quartz particles of the same size to achieve isothermal operation. The temperature in the middle of the catalytic bed was measured with a coaxial thermocouple. The samples were activated in flowing oxygen at 450 °C for 30 min. The composition of the reaction mixture was 9.1% C_2H_6/9.1% O_2/81.8% He.

The oxidative dehydrogenation of ethane was investigated in the temperature range 300–425 °C. For the determination of the activity of the catalysts as a function of temperature, the W/F ratio was kept constant at 0.54 g s/cm^3. To obtain different ethane conversion levels at constant reaction temperature (350 °C), the W/F ratio was varied from 0.02 to 1.73 g s/cm^3. The stability of the catalyst with the optimum composition was studied by continuously recording the catalytic performance for 24 h on line at constant reaction conditions ($T = 350$ °C; $W/F = 0.54$ g s/cm^3).

The reaction products were analyzed on line by a Perkin Elmer gas chromatograph equipped with a thermal conductivity detector. Two columns in a series-bypass configuration were used in the analysis, a Porapak Q and an MS 5A. The main reaction products were C_2H_4, CO_2, and H_2O. Negligible amounts of oxygenates were observed at the reactor exit. Ethane conversion and selectivity to the reaction products were calculated on a carbon basis. Closure of the carbon mass balance was better than ±1%. The contribution of gas-phase-initiated reactions was tested by conducting experiments using an empty-volume reactor. The conversion of ethane at these experiments was <1%, confirming that gas-phase reactions are negligible at the experimental conditions used for the activity tests.

3. Results

3.1. Catalyst characterization

The composition and the main physicochemical characteristics of the Ni–Nb–O mixed oxides are presented in Table 1. The surface area recorded for NiO was relatively low, but increased considerably upon introduction of Nb. This increase can be attributed to the use of niobium oxalate as starting compound for Nb. The decomposition (during calcination) of precursors with organic nature yields a more porous structure than for the inorganic nitrate salts used for nickel oxide preparation. A maximum surface area is recorded for the $Ni_{0.85}Nb_{0.15}$ catalyst, whereas a significant reduction is recorded for $Ni_{0.6}Nb_{0.4}$, due to the extended phase segregation and formation of large Nb_2O_5 crystallites (see the XRD results).

XRD was used to investigate the crystalline phases formed in the calcined catalysts. Fig. 1 illustrates the diffractograms obtained for all of the samples, plus that of NiO and Nb_2O_5 used as references. Catalysts with Nb content up to 15% relative to the total metal content exhibit only the diffraction lines corresponding to a crystalline "NiO-like" phase, with a broad band centered at 2θ 27° attributed to an amorphous niobium phase. By only slightly increasing the Nb content (catalyst $Ni_{0.8}Nb_{0.2}$) only slightly, sharp diffractions lines at 2θ 35.9°, 41°, and 53.8° indicate the formation of the mixed $NiNb_2O_6$ phase. In the

Table 1
Nomenclature and physicochemical characteristics of the catalysts

Sample	Nb/Ni atomic ratio	NiO loading (wt%)	Surface area (m^2/g)	NiO average crystal size (nm)	NiO lattice constant (Å)	Acidity (μmol_{NH_3}/m^2)
NiO	0	100	16.7	31.8	4.1762	0.92
$Ni_{0.9}Nb_{0.1}$	0.111	83.49	55.9	21.4	4.1751	3.30
$Ni_{0.85}Nb_{0.15}$	0.176	76.10	85.1	16.7	4.1725	3.44
$Ni_{0.8}Nb_{0.2}$	0.250	69.21	58.6	14.3	4.1722	3.18
$Ni_{0.7}Nb_{0.3}$	0.428	56.74	57.1	14.9	4.1723	3.13
$Ni_{0.6}Nb_{0.4}$	0.666	45.74	31.4	21.6	4.1721	2.95
Nb_2O_5	–	0	32.5	–	–	5.04

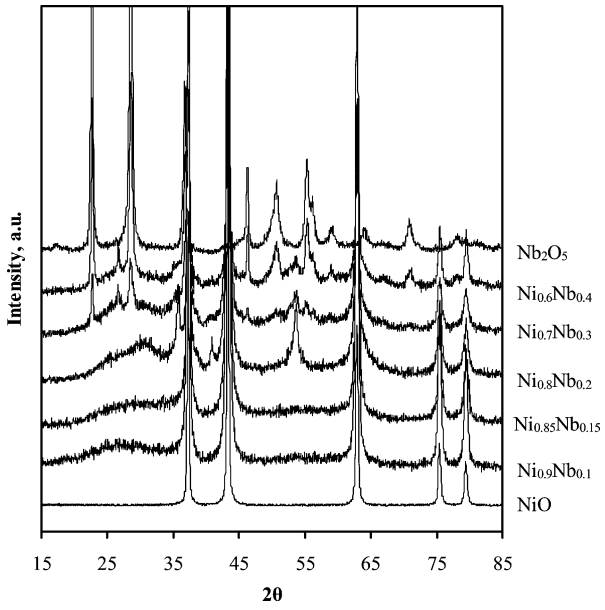

Fig. 1. X-Ray diffraction patterns of the Ni–Nb–O catalysts and reference materials NiO and Nb_2O_5.

high-Nb content catalysts ($Ni_{0.7}Nb_{0.3}$ and $Ni_{0.6}Nb_{0.4}$), the intensity of the $NiNb_2O_6$ lines drops and crystalline Nb_2O_5 is detected.

Analysis of the XRD patterns allowed the calculation of particle size and lattice parameters of the nickel oxide-like phase in the as synthesized mixed oxides, presented in Table 1. The XRD analysis shows that pure NiO crystallizes in the cubic rock salt structure with a lattice constant of $a = 4.1762$ Å, in agreement with reported data (JCPDS 4-835). The incorporation of Nb causes a contraction of the NiO lattice, as evidenced by the monotonous decrease of the lattice constant with increasing Nb content (Table 1) up to a Nb/Ni ratio of 0.176. Further increase of the niobium amount does not cause other alterations, and the lattice constant remains invariable. This observed decrease in the size of the NiO unit cell could be discussed in terms of a possible substitution of some of the host cations (Ni^{2+}) by the foreign species (Nb^{5+}). The substitution process requires that the ionic radii of host and foreign cations be similar. The ionic radii of Ni^{2+} and Nb^{5+} are 0.69 Å [20] and 0.64 Å, respectively; therefore, a substitution between the two cations is possible and would lead to a reduction of the lattice constant, since the radii of Nb^{5+} is smaller than that of Ni^{2+}. The results of the XRD analysis support this notion. This substitution process also leads to charge imbalance due to the different valency of the nickel and niobium cations, which significantly modifies the properties of the mixed Ni–Nb–O oxides, as discussed in detail later in the paper. The stable NiO lattice constant measured for the high-Nb loading samples ($Ni_{0.8}Nb_{0.2}$, $Ni_{0.7}Nb_{0.3}$, and $Ni_{0.6}Nb_{0.4}$) indicates that we have reached an upper limit to the maximum possible dissolution of Nb^{5+} cations into the NiO lattice.

Based on the foregoing, the "NiO-like" phase detected in the diffractograms of the Ni–Nb–O mixed oxides can be identified as a Ni–Nb solid solution. The highest proportion of this solid solution is obtained for the $Ni_{0.85}Nb_{0.15}$ compound, whereas segregation phenomena occur between Nb_2O_5 and NiO phases for Nb/Ni atomic ratios >0.176. Additional information deduced from the XRD analysis is that the Ni–Nb–O mixed oxides consist of crystallites in the nanorange and thus can be classified as nanomaterials. Clearly, crystallite size is always smaller for the mixed oxides than for the pure oxides. This phenomenon can be explained by the increased crystallographic disorder in the Ni–Nb–O catalysts, which could also be responsible for the high surface area recorded for the catalyst with the highest proportion of the Ni–Nb solid solution ($Ni_{0.85}Nb_{0.15}$). The crystal size reaches a minimum for an intermediate Nb/Ni ratio equal to 0.25 and increases with further increasing Nb content. The incorporation of niobium in the nickel oxide lattice inhibits crystallization, and thus smaller grain sizes are recorded. However, at high Nb loading and as the two phases (NiO and Nb_2O_5) begin to segregate, crystallization of NiO occurs more freely, leading to the detection of larger crystals. The same effect has been reported for $CeNi_xO_y$ mixed oxides [21].

The surface morphology of the synthesized materials was examined by SEM. Micrographs of the Ni–Nb–O mixed oxides of all compositions, together with those of the NiO and Nb_2O_5 reference compounds, are presented in Figs. 2A–2G. Pure nickel oxide consists of well-defined cubic microcrystallites in the nanosize range, in full agreement with the XRD results. The addition of niobium induces significant changes in morphology. The $Ni_{0.9}Nb_{0.1}$ and $Ni_{0.85}Nb_{0.15}$ samples show homogeneous particles with a sponge-like appearance, reflecting the lower crystallinity and higher surface area detected by the previous characterization techniques and consistent with the formation of a Ni–Nb solid solution. The EDS analysis revealed a highly homogeneous elemental distribution of Ni and Nb on these catalysts, as shown in Fig. 3A for $Ni_{0.85}Nb_{0.15}$, with the Nb/Ni atomic ratio centered on the nominal value. Further increase in Nb loading leads to the formation of few larger plate-like crystallites ($Ni_{0.8}Nb_{0.2}$ catalyst; Fig. 2D), whereas on the high-Nb content samples ($Ni_{0.7}Nb_{0.3}$ and $Ni_{0.6}Nb_{0.4}$), a clear change of the surface morphology is apparent. The particles of sponge-like appearance disappear, and the catalysts consist of well-defined plate-like crystallites, corresponding to the Ni–Nb phase, and smaller round white particles, corresponding to pure Nb_2O_5, as confirmed by the elemental EDS analysis presented in Fig. 3B for the $Ni_{0.6}Nb_{0.4}$ oxide.

The reducibility of the catalysts was studied with TPR in H_2. The TPR profiles, shown in Fig. 4, were acquired by continuously following the H_2 signal with a quadrupole mass spectrometer while linearly increasing temperature. Pure NiO exhibits a relatively narrow reduction peak with a maximum at 415 °C. Calculation of the consumed hydrogen indicates total reduction of Ni^{2+} ions to metallic Ni. The introduction of Nb significantly broadens the reduction profiles, indicating modification of the catalysts and contributions from different species. The main reduction peak is shifted to 390 °C in $Ni_{0.9}Nb_{0.1}$, and a broad shoulder centered at 500 °C appears. The same profile, shifted about 30 °C lower, is also recorded for the $Ni_{0.85}Nb_{0.15}$ catalyst. In $Ni_{0.8}Nb_{0.2}$ we observe two distinct peaks with maxima at 340 °C and 460 °C, ascribed to two well-defined reducible species. In view of the XRD results,

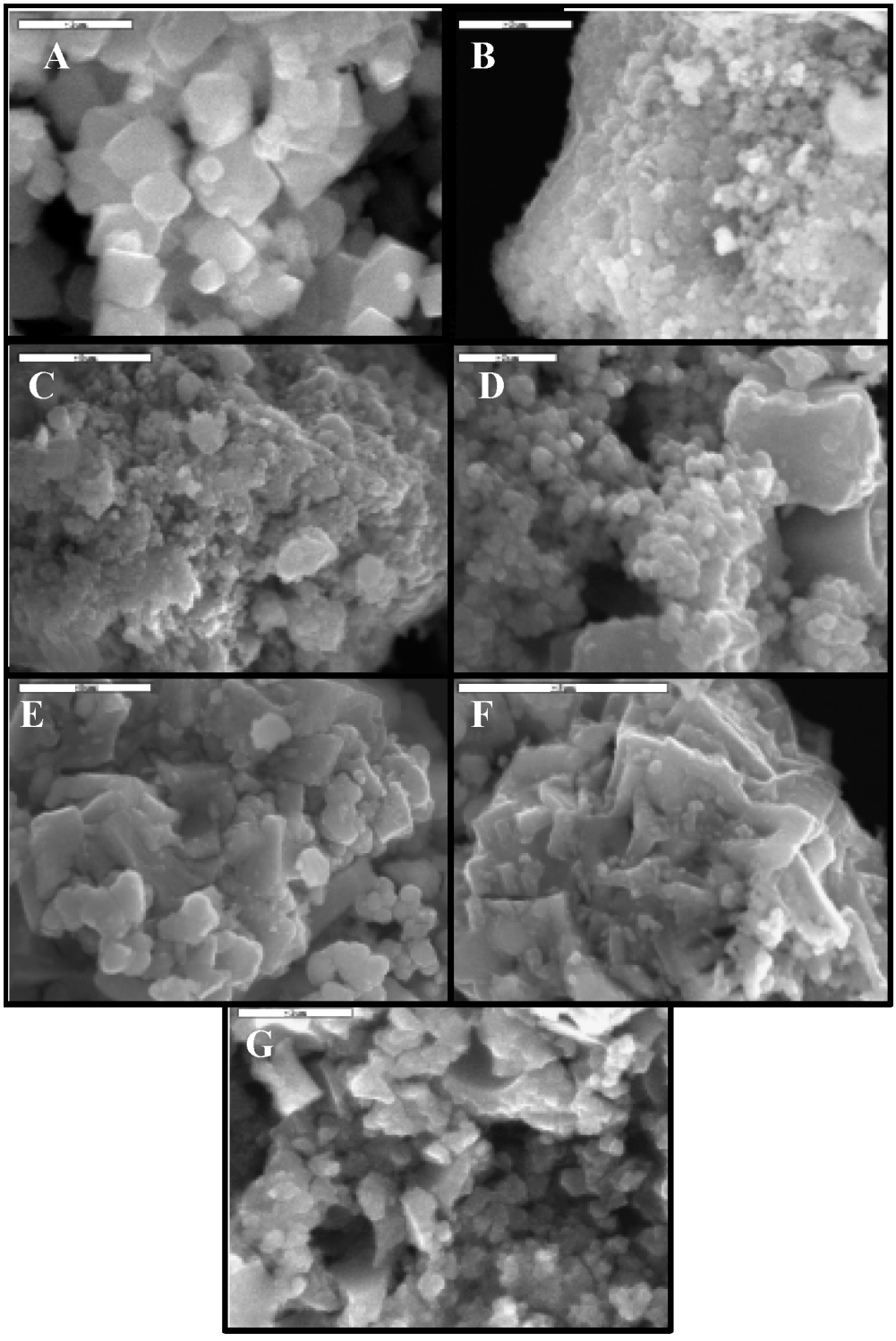

Fig. 2. SEM micrographs of the Ni–Nb–O catalysts and reference materials NiO and Nb_2O_5: (a) NiO; (b) $Ni_{0.9}Nb_{0.1}$; (c) $Ni_{0.85}Nb_{0.15}$; (d) $Ni_{0.8}Nb_{0.2}$; (e) $Ni_{0.7}Nb_{0.3}$; (f) $Ni_{0.6}Nb_{0.4}$; (g) Nb_2O_5.

this second peak can be attributed to the crystalline $NiNb_2O_6$ phase, detected only in this sample. This observation is also in line with literature data reporting the reduction temperature of bulk nickel niobate to be around 480 °C [22]. The catalysts with 70 and 60% Ni present similar reduction characteristics, with a single rather narrow peak shifted to ∼360 °C. A very small shoulder evident near 500 °C could be due to minor amounts of $NiNb_2O_6$ still present in the high-Nb loading samples.

Quantification of the TPR curves shows that hydrogen consumption is linearly dependent on the wt% amount of NiO in the catalysts, as graphically illustrated in Fig. 5, and corresponds to the total reduction of Ni ions from +2 to the metallic form. Given that Nb_2O_5 is irreducible under the conditions used

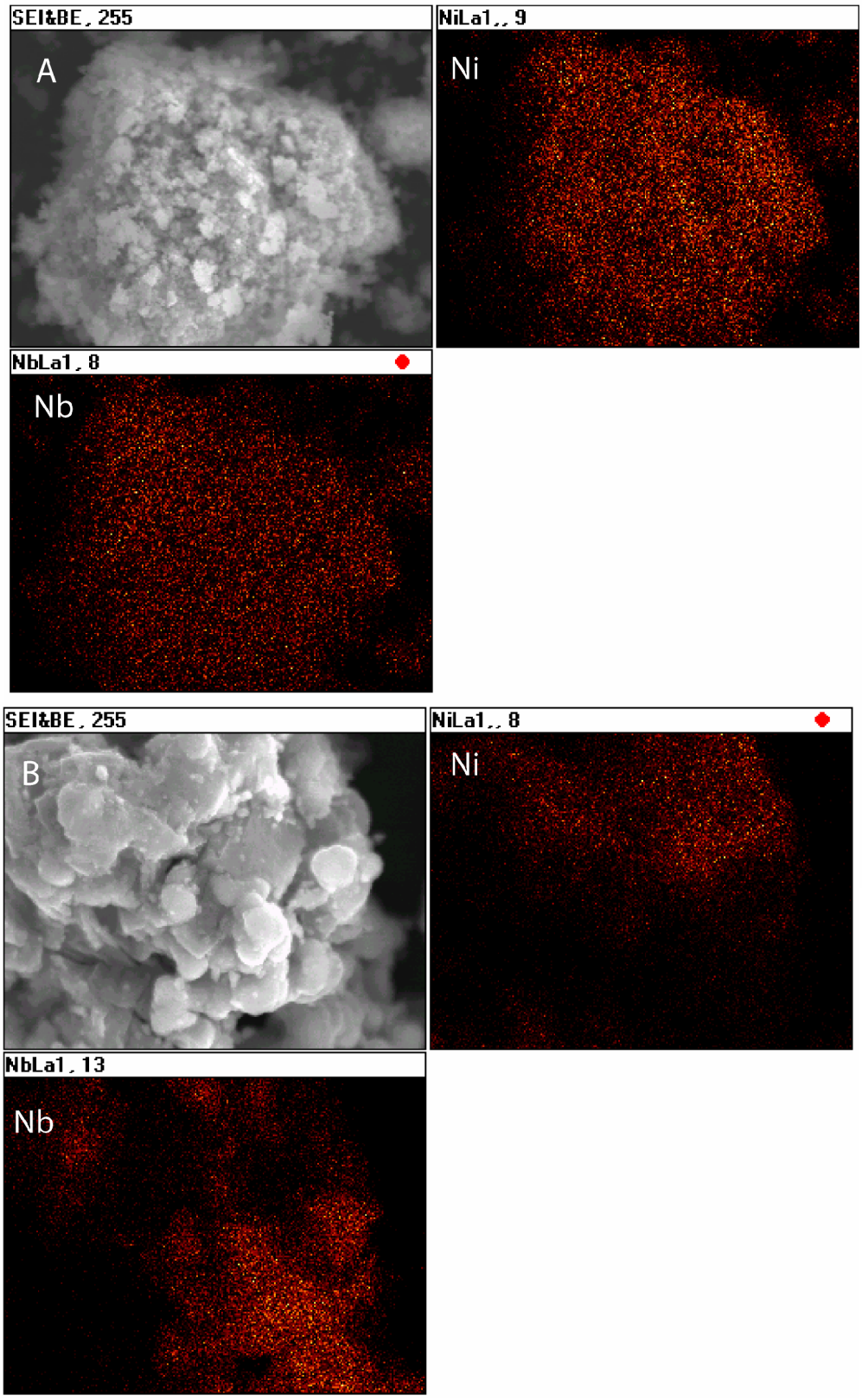

Fig. 3. SEM micrographs and corresponding EDS elemental analysis of niobium and nickel for (a) $Ni_{0.85}Nb_{0.15}$; (b) $Ni_{0.6}Nb_{0.4}$.

in the TPR measurements (evidenced by testing of the pure niobium oxide), reduction of the catalysts thus occurs by removal of oxygen from Ni–O–Ni and Ni–O–Nb bonds. Nb incorporation weakens the Ni–O–Ni bonds, because the oxygen can be removed at lower temperatures than in pure NiO. Based on the electronegativity concept, the presence of niobium in the coordination sphere of nickel should decrease the electronic density of nickel (Pauling electronegativity of 1.9 for Ni and 1.6

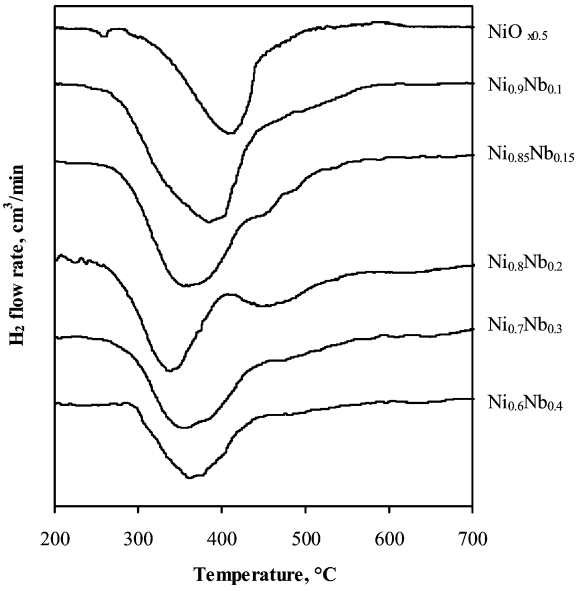

Fig. 4. Temperature-programmed reduction profiles of the Ni–Nb–O catalysts and reference material NiO.

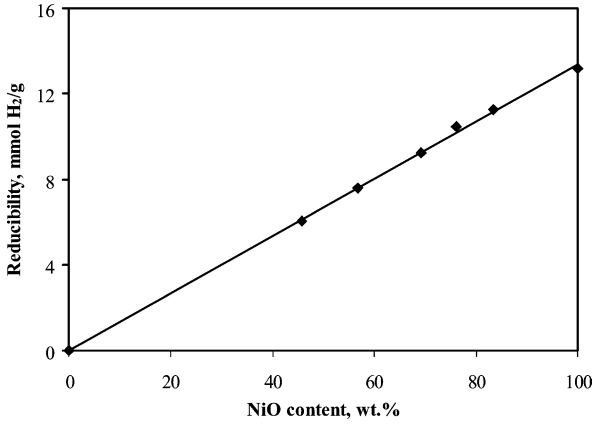

Fig. 5. Hydrogen consumption versus wt% NiO loading.

for Nb), and thus facilitate its reduction. The high-temperature shoulders in the TPR patterns can be ascribed to the reduction of formed Ni–O–Nb bonds. The absence of such extended high temperature reduction in the high-Nb content samples (30 and 40% Nb) is consistent with the preferential formation of niobium oxide, Nb–O–Nb bonds that are irreducible, at the expense of the formation of Ni–O–Nb heterolinkages. The TPR results are analogous to reducibility results obtained with NiO/Al_2O_3 and $Ni–Nb/Al_2O_3$ catalysts presented in our previous work [13], where the promotion with Nb caused the appearance of two reduction peaks, one at lower temperature and one at higher temperature than the Nb-free sample attributed to reduction of Ni–O–Ni and Ni–O–Nb bonds, respectively.

Acidity was determined by TPD after saturation of the catalytic surface with ammonia at 100 °C. In all cases the main desorption product was NH_3, with traces of N_2, NO, and N_2O also detected. The ammonia desorption curves are compiled in Fig. 6, and the acidity of the catalysts (expressed as μmol of desorbed NH_3/m^2) is tabulated in Table 1. Pure NiO exhibits very low acidity, with a small peak appearing at high temperature (700 °C) in the TPD profile. The introduction of niobium causes a significant increase in the total acidity and generates new acid sites of weak and moderate strength. The Ni–Nb–O mixed oxides are characterized by a narrow desorption peak in the range 130–450 °C, with maximum temperature of desorption at 220–230 °C. Although mild differences between the different catalyst compositions are seen, acidity increases with increasing Nb content, reaches a maximum for a Nb/Ni ratio of 0.176, and decreases slightly at higher Nb concentrations. Pure Nb_2O_5 has the highest total surface acidity, exhibiting a similar TPD profile as the catalysts. It is well known that niobium oxide has high acidic properties, with the Lewis acid sites corresponding to highly distorted NbO_6 octahedra [23].

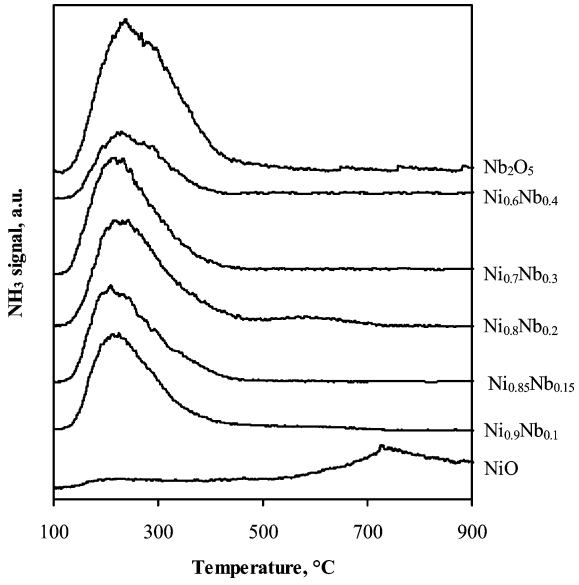

Fig. 6. Ammonia desorption curves of the Ni–Nb–O catalysts and reference materials NiO and Nb_2O_5.

In summary, the acidic measurements show that the Ni–Nb–O mixed oxides exhibit high moderate acidity, much higher than the sum of the acidity of the individual components in each catalytic composition. The effect is much more pronounced if we compare, for example, pure NiO and the $Ni_{0.9}Nb_{0.1}$ catalyst, where the introduction of only 10% of Nb leads to an almost 300% increase in acidity. According to a model described by Tanabe [24], the substitution of cations M^{n+} of a host oxide by cations N^{m+} of another metal oxide can generate acidic centers due to the charge imbalance along M–O–N linkages. This acidity is defined as Brønsted or Lewis based on whether this excess charge is negative or positive, respectively. The model structure postulates that each cation retains its parent coordination number, whereas all oxygen anions in the binary oxide maintain the coordination of the major component oxide. The application of these assumptions to the $NiO–Nb_2O_5$ system explains the remarkable increase in acidity exhibited by the Ni–Nb–O catalysts compared to pure nickel oxide. Bulk NiO is a well-known nonstoichiometric oxide with cationic vacancies [25]. Therefore, the filling of the cationic vacancies and/or the substitution of Ni^{2+} ions by Nb^{5+} in the NiO lattice creates an excess positive charge along the Ni–O–Nb linkages, and thus

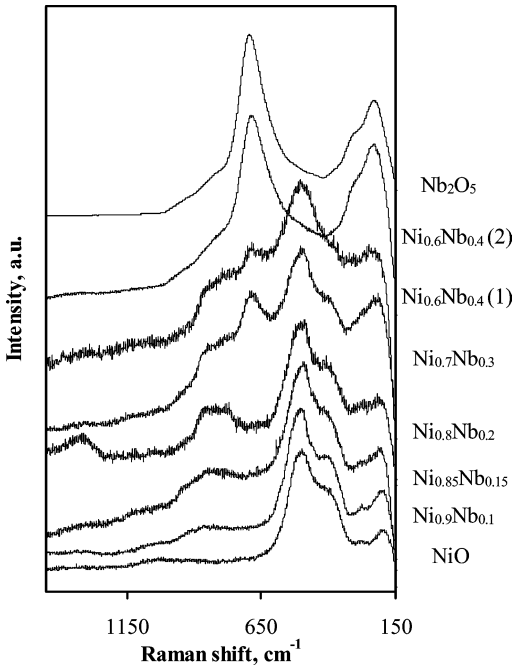

Fig. 7. Raman spectra of the Ni–Nb–O catalysts and reference materials NiO and Nb_2O_5.

the mixed oxide should exhibit high Lewis acidity. As already discussed, the acidity reaches a maximum for the $Ni_{0.85}Nb_{0.15}$ catalyst and then decreases slightly for higher Nb content. The XRD data indicate, based on the calculated NiO lattice constant, that maximum solubility of niobium cations in NiO is attained for the same catalyst ($Ni_{0.85}Nb_{0.15}$), confirming that the observed acidity is related to the formation of Ni–O–Nb bonds. A further increase in the Nb/Ni ratio results in extended segregation of the NiO and Nb_2O_5 phases and, consequently, in fewer Ni–O–Nb bonds and relatively reduced acidity.

Raman spectra of the Ni–Nb–O mixed oxides collected at ambient conditions are presented in Fig. 7, including the spectra of reference NiO and Nb_2O_5 compounds. NiO exhibits a strong band at 500 cm^{-1} due to the Ni–O stretching mode, with a shoulder at 410 cm^{-1} indicative of the nonstoichiometry of the material [20] and the high nickel vacancy concentration. The Raman spectrum of Nb_2O_5 exhibits two strong features at 695 and 235 cm^{-1}, with a shoulder appearing at 310 cm^{-1} and a broad band in the 800–1000 cm^{-1} range. Niobium pentoxide generally has an octahedrally coordinated NbO_6 structure that is distorted to varying extents depending on whether its polyhedra are corner- or edge-shared. Highly distorted NbO_6 octahedra have Nb=O bonds, whereas the slightly distorted ones have only Nb–O bonds [26]. The band at 695 cm^{-1} is assigned to the symmetric stretching mode of the niobia polyhedra, and its position and sharpness reveals an ordered structure and an increasing bond order of the [NbO_6] units, crystallized in the pseudohexagonal phase (TT-Nb_2O_5). The Raman bands in the low-wavenumber region, 200–300 cm^{-1}, are characteristic of the bending modes of the Nb–O–Nb linkages, whereas the additional weak band centered at ∼900 cm^{-1} is due to a small concentration of the Nb=O surface sites of highly distorted octahedra [27].

Table 2
Nominal and surface atomic composition (derived from XPS) of the catalysts

Sample	Nominal composition (%)			Surface composition (%)		
	Ni	Nb	O	Ni	Nb	O
NiO	50	–	50	46.06	–	53.94
$Ni_{0.9}Nb_{0.1}$	42	5	53	39.90	6.05	54.64
$Ni_{0.85}Nb_{0.15}$	38	7	55	39.61	6.51	54.50
$Ni_{0.8}Nb_{0.2}$	35	9	57	38.08	7.63	55.03
$Ni_{0.7}Nb_{0.3}$	29	12	59	40.01	6.04	54.53
$Ni_{0.6}Nb_{0.4}$	23	15	62	25.44	13.96	62.14

The introduction of Nb in NiO with a Nb/Ni atomic ratio of 0.111 results in the appearance of a weak broad band centered at ∼850 cm^{-1}, in addition to the features of NiO. With increasing Nb content, this band becomes more intense and shifts to 840 cm^{-1} for the $Ni_{0.85}Nb_{0.15}$ catalyst. In the spectrum of the $Ni_{0.8}Nb_{0.2}$ catalyst, this feature develops into a well-defined band, red-shifted to 800 cm^{-1}. The nature of surface NbO_x species supported on several carriers (SiO_2, Al_2O_3, ZrO_2, TiO_2) has been investigated in detail by Raman and infrared spectroscopy by Wachs and co-workers [28]. According to this study, vibrations of Nb=O bonds of monomeric and polymeric niobia species generally occur at wavenumbers above 950 cm^{-1}; therefore, the broad band detected in the 950–750 cm^{-1} range in our samples cannot be assigned to any possible surface niobia structures on nickel oxide having niobium–oxygen double bonds. Lower frequency vibrations in the 850–950 cm^{-1} range have been attributed to symmetric stretchings of $[–O–Nb–O–]_n$ bonds [28]. It is thus possible that the broad bands observed on the Raman spectra of the Ni–Nb–O mixed oxides result from vibrations of bridging Nb–O–Nb bonds of surface species or/and vibrations of bridging Ni–O–Nb bonds located on the surface of the NiO structure.

Additional bands originating from well-ordered crystalline [NbO_6] polyhedra appear at 695 and 235 cm^{-1} in the spectra of the $Ni_{0.7}Ni_{0.3}$ and $Ni_{0.6}Nb_{0.4}$ catalysts, indicating the crystallization of niobium in the pure oxide form in agreement with the XRD results. Moreover, it should be mentioned that the $Ni_{0.6}Nb_{0.4}$ sample is highly inhomogeneous and Raman spectra acquired from white particles in the sample are identical to that of pure Nb_2O_5 (spectrum shown in Fig. 7), confirming the significant formation of pure niobium oxide crystals detected by XRD and EDX analysis.

The surface composition of the mixed nickel–niobium oxides was determined by XPS, because this technique has a surface-specific character and allows quantitative determination of the elemental content in the upper layers of the sample. The nominal and surface atomic composition of the synthesized catalysts is presented in Table 2. The values of the surface composition were derived from the integration of the Ni 2p, Nb 3d, and O 1s core-level photoemission spectra, using the appropriate sensitivity correction factors. Concerning pure NiO, a nickel atom deficiency and an excess concentration of oxygen on the surface is apparent, consistent with the Raman indications and the general consensus in literature about the nonstoichiometric nature of NiO [20,25]. Furthermore, the color of the sample (gray) is also proof of the nonstoichiometry of the material,

because stoichiometric NiO is green. In the series of the Ni–Nb–O catalysts with varying Nb/Ni ratio, the surface compositions for Nb/Ni ratios from 0.11 to 0.43 (catalysts $Ni_{0.9}Nb_{0.1}$, $Ni_{0.85}Nb_{0.15}$, $Ni_{0.8}Nb_{0.2}$, and $Ni_{0.7}Nb_{0.3}$) appear similar irrespective of the different nominal content, leading to an average Ni surface coverage of 40% and an average Nb surface coverage of 6.5%. This observation is in agreement with our previous results on promoted-Ni/Al_2O_3 catalysts [13], where the preferential exposure of the promoter or the nickel on the surface was found to depend largely on the surface energy, not the composition, of the respective oxides. Therefore, in multicomponent systems the surface composition is the result of a thermodynamic driving force, according to which surface acquires the composition that leads to the lowest possible surface energy. Thus, the similar surface compositions detected for four of the five catalysts indicates that this preferential surface exposure of nickel and niobium in a fixed analogy, independent of the nominal content, is energetically the most favorable arrangement of the surface. Only the catalyst with the highest Nb content, the $Ni_{0.6}Nb_{0.4}$ catalyst, constitutes an exception to the above, with the surface composition approaching the nominal values. This could be due to the severe segregation and formation of crystals of the independent oxides that was detected on this sample, as well as the sample's high inhomogeneity (Figs. 2F and 3B).

Electrical conductivity measurements carried out on oxide-based catalysts can provide valuable information on the nature of structural defects, the existence of oxidizing species, and so on [29]. Furthermore, investigating the electrical properties provides important insights, particularly in the case of redox reactions, because these properties are closely related to the nature and reactivity of the oxygen species formed on activation of the oxidant (O_2) on the catalytic surface. Numerous previous studies have correlated the catalytic performance of metal oxide catalysts in partial oxidation reactions with the conductivity of the oxide materials, for example, ethane to ethene [30,31], propane to propene [32–34], *n*-butane to butenes [35,36], and butane to maleic anhydride [37].

The DC electrical conductivity of the Ni–Nb–O mixed oxides and of pure nickel and niobium oxide at room temperature is plotted as a function of the Nb/Ni atomic ratio in Fig. 8. NiO exhibits high conductivity, in accordance with data reported previously [38]. Doping of NiO with even the smallest amount of Nb ($Ni_{0.9}Nb_{0.1}$ catalyst) causes a decrease in conductivity by more than an order of magnitude. Further increases in Nb loading do not cause significant alterations, with a slight decreasing trend with increasing Nb content leading to the very small value exhibited by pure Nb_2O_5 (two orders of magnitude lower than NiO).

As mentioned earlier, bulk NiO is a well-known p-type semiconductor with conductivity attributed to cation deficiency [39,40], justifying the high value recorded for pure NiO. The cationic vacancies induce the formation of positive holes p^+, the main charge carriers, which are introduced in the form of Ni^{3+} or O^- ions to maintain charge neutrality conditions [41,42]. Concerning the Ni–Nb–O catalysts, the formation of a Ni–Nb solid solution, suggested by previous characterization techniques, is directly confirmed by the conductivity measurements. From an electrical standpoint, the dissolution of heterovalent ions in the lattice of a host oxide creates free charge carriers (electrons or holes) to maintain electrical neutrality. The dissolution of higher valence cations, such as Nb^{5+}, in the p-type NiO lattice suggests an *n*-doping character of Nb. Niobium oxide is an *n*-type semiconductor with nonstoichiometry arising from a lack of oxygen ions and free electrons as main charge carriers. Therefore, niobium acts as a donor of electrons and fills the electron (hole) states on Ni, thereby reducing the positive hole p^+ concentration and, consequently, the conductivity compared with pure NiO, consistent with our results.

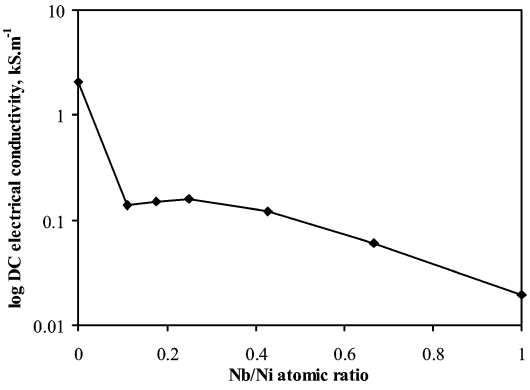

Fig. 8. DC electrical conductivity measured at ambient conditions versus Nb/Ni atomic ratio.

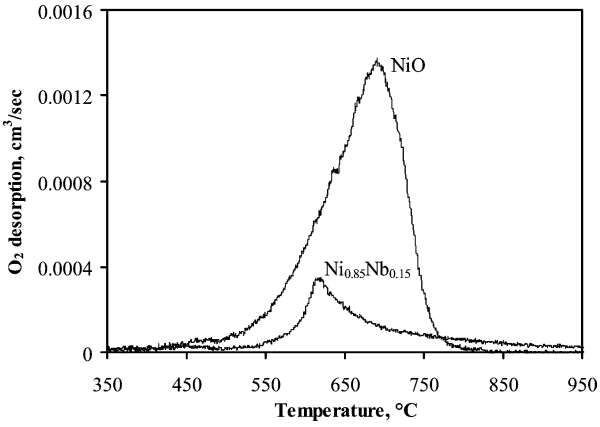

Fig. 9. Temperature-programmed oxygen desorption curves of NiO and $Ni_{0.85}Nb_{0.15}$ catalyst.

Based on the nonstoichiometry and consequent high conductivity of NiO, the presence of electrophilic oxygen radicals (O^-) on the NiO surface is expected. Indeed, NiO has been reported to accommodate a large amount of surface excess oxygen [38]. As shown earlier, the incorporation of Nb ions in the NiO lattice reduces the p^+ concentration and thus should reduce the amount of excess oxygen that the surface can accommodate. To verify this hypothesis, we performed O_2-TPD measurements on pure NiO and the $Ni_{0.85}Nb_{0.15}$ catalyst, which, according to the characterization results, has the highest proportion of the Ni–Nb solid solution. The profiles of oxygen desorption with increasing temperature are compiled in Fig. 9. Indeed, NiO exhibits a large oxygen desorption peak in the 450–850 °C range, with maximum temperature of desorption

at 695 °C, in agreement with O_2-TPD measurements on NiO reported previously [15]. The amount of oxygen desorbed corresponds to a 1.14% excess of oxygen (mol) per mole of NiO. It has been reported previously that oxygen desorption from NiO occurring at temperatures below 700 °C corresponds to the nonstoichiometric oxygen [43]. For the Nb/NiO catalyst, a much smaller desorption peak, asymmetric on the high-temperature side, is recorded, with a T_{max} of desorption at 625 °C. The desorbed oxygen amounts to only a 0.2% excess of oxygen per mole of catalyst, clearly confirming that the introduction of Nb minimizes the nonstoichiometry of the material, fills the NiO cationic vacancies, and reduces the chemisorbed oxygen species on the catalytic surface. It should be noted that repetition of the O_2-TPD experiments without prior O_2 adsorption yielded the same desorption patterns. This, in combination with the absence of low-temperature oxygen desorption peaks, indicates that NiO and the Nb-doped NiO materials do not adsorb oxygen at the experimental conditions used in this study (ambient conditions), and that the desorbed oxygen originates from the bulk structure of the materials under study.

3.2. Catalytic performance in ethane ODH

The activity of the Ni–Nb–O mixed oxide catalysts in the ethane oxidative dehydrogenation reaction was explored under steady-state conditions at 300–425 °C with a constant W/F (0.54 g s/cm^3) and ethane-to-oxygen ratio (1/1). Ethane conversion is plotted as a function of temperature in Fig. 10. Note that in all cases, oxygen conversion did not exceed 90%. Generally, all tested catalysts prove to be very reactive, effectively converting ethane at low reaction temperatures. The incorporation of even small amounts of Nb (Nb/Ni = 0.111) in NiO causes a 100% increase in the per weight reactivity compared with the pure nickel oxide. Increasing the Nb content in the mixed oxides leads to increased ethane conversion, which reaches a maximum for the $Ni_{0.85}Nb_{0.15}$ catalyst (66% C_2H_6 conversion at 400 °C). Further increases result in a decline in reactivity, which still, however, remains higher than that of pure NiO, except for the highest-Nb loading catalyst ($Ni_{0.6}Nb_{0.4}$), in which a sharp decrease is observed. Pure Nb_2O_5 oxide tested under the same reaction conditions exhibited negligible activity (<1% ethane conversion) at 300–450 °C, with ethene selectivity not surpassing 65% even at this low conversion levels.

To account for the different surface areas of the samples, the activity of the catalysts in terms of specific surface activity (SSAc)—expressed as μmol C_2H_6 consumed/(m^2 s)—was also considered. Based on this definition, the reactivity of the tested catalytic materials at 300 °C decreased in the following order: NiO > $Ni_{0.85}Nb_{0.15}$ > $Ni_{0.9}Nb_{0.1}$ > $Ni_{0.8}Nb_{0.2}$ > $Ni_{0.7}Nb_{0.3}$ > $Ni_{0.6}Nb_{0.4}$. Pure NiO now exhibits a higher surface reactivity for ethane activation compared with the Ni–Nb–O oxides, due to the large increase of the surface area on incorporation of Nb (which thus lowers the surface activity of the catalysts). However, as shown in the next paragraph, ethane activation on NiO is unselective, leading to combustion (see Section 4). The activity trend is maintained for the Ni–Nb–O catalysts, with optimum reactivity exhibited by Nb/Ni ratios of 0.111–0.176.

The most important requirement for a good ODH catalyst is the ability to effectively convert ethane to ethylene at low temperature with high selectivity. To study the selectivity of the mixed Ni–Nb–O oxides, and since selectivity is generally strongly related to conversion, we conducted a second series of experiments at constant temperature (350 °C), constant ethane/oxygen ratio (1/1), and varying W/F (0.02–1.73 g s/cm^{-3}), to attain different conversion levels. Ethylene selectivity as a function of ethane conversion is presented in Fig. 11. The most prominent feature is the enormous increase of ethene selectivity upon incorporation of Nb, climbing from 20% for NiO to 80% for the lowest Nb content catalyst ($Ni_{0.9}Nb_{0.1}$). Varying the Nb/Ni ratio leads to a maximum in selectivity for the $Ni_{0.85}Nb_{0.15}$ catalyst (90%), with further Nb increases decreasing selectivity slightly, down to 80% for $Ni_{0.6}Nb_{0.4}$. Overall, all Ni–Nb–O catalysts demonstrate excellent ability to selectively convert ethane to ethylene. It is also of great importance that selectivity remains virtually constant with increasing ethane conversion at 350 °C for the conversion range studied (0–20%). The main problem with ODH catalysts is the secondary overoxidation of the alkene produced, which causes the drop in selectivity with increasing conversion. These mate-

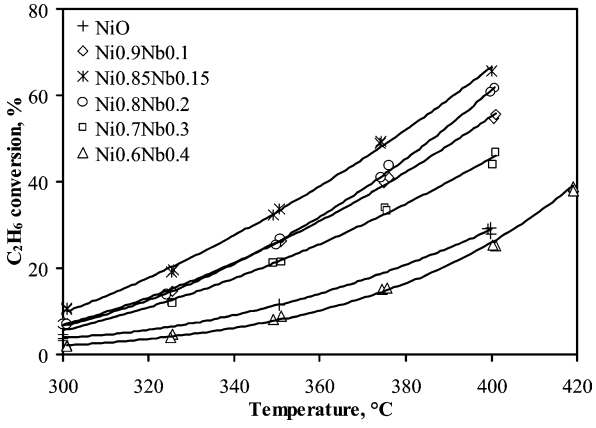

Fig. 10. Ethane conversion as a function of temperature (reaction conditions: $W/F = 0.54$ g s/cm^3, $C_2H_6/O_2 = 1/1$).

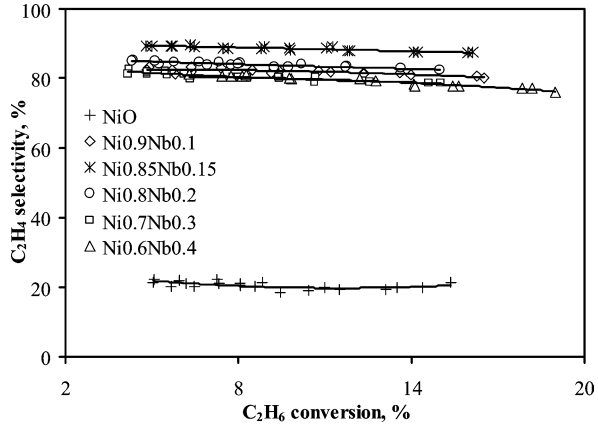

Fig. 11. Ethene selectivity as a function of ethane conversion (reaction conditions: $T = 350$ °C, $C_2H_6/O_2 = 1/1$).

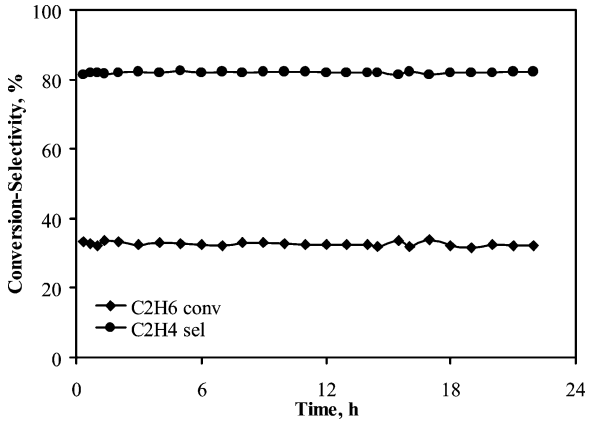

Fig. 12. Ethane conversion and ethene selectivity as a function of TOS (reaction conditions: $T = 350\,^{\circ}\mathrm{C}$, $W/F = 0.54\ \mathrm{g\,s/cm^3}$, $C_2H_6/O_2 = 1/1$).

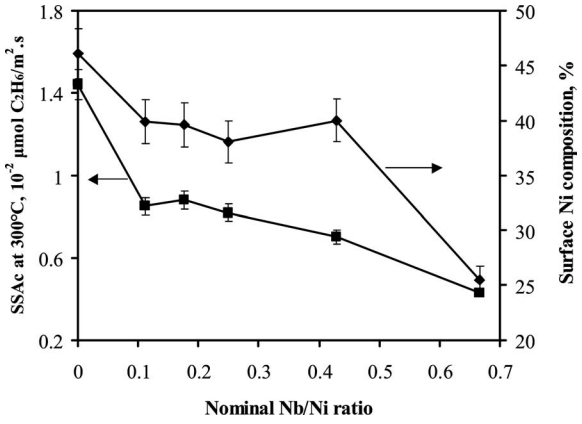

Fig. 13. Specific surface activity (SSAc) in ethane ODH and surface Ni content versus nominal atomic Nb/Ni ratio.

rials exhibit very stable ethene selectivity, indicating that they are very reactive toward ethane but have a very low affinity to ethylene, thus preserving the olefin from further oxidation. Another important advantage of the Ni–Nb–O catalysts is that the only byproduct detected is CO_2, resulting from primary unselective oxidation of ethane.

Stability is a very important parameter that often defines the "fate" of a specific catalytic material for potential industrial application. In a final step, the stability of the catalyst with the optimum formulation, the $Ni_{0.85}Nb_{0.15}$ oxide, was investigated by continuously recording the catalytic performance for 24 h on-line at constant reaction conditions ($T = 350\,^{\circ}\mathrm{C}$) and high ethane conversion levels. The results of the stability test, presented in Fig. 12, clearly show the high stability of the catalytic materials, with both ethane conversion and ethylene selectivity maintaining their initial values for the entire time span of the experiment, which, although shorter than what is typically required for commercial application, demonstrates the high potential of the mixed Ni–Nb–O catalysts.

4. Discussion

Ni–Nb–O mixed oxides prove to be highly active and selective catalytic materials for the production of ethene via ethane oxidative dehydrogenation, exhibiting an overall ethylene yield of 46% at 400 °C. In comparison with the alumina-supported Ni–Nb mixed oxide catalyst recently presented in one of our previous work [13], the binary Ni–Nb–O mixed oxides exhibit an impressive improvement (160%) in ethene yield. Furthermore, the Ni–Nb–O materials compare favorably with most ODH catalysts reported in the literature. A summary of performance data for a wide variety of catalytic systems in terms of selectivity for ethene as a function of ethane conversion and reaction temperature is available elsewhere [1]. Most catalysts either exhibit high initial selectivity, which quickly drops with increasing conversion, or demand high reaction temperatures for achieving acceptable yields. The developed Ni–Nb–O catalysts for ethane ODH presented in this study appear to be clearly superior, combining high activity at low temperature and high ethene selectivity at high conversion levels (66% C_2H_6 conversion and 70% C_2H_4 selectivity at 400 °C), with very stable catalytic performance. A further advantage of these catalysts is that the only byproduct detected was CO_2, making these materials very attractive from an engineering standpoint because of the greatly reduced separation costs downstream from the reactor in any potential industrial application of an oxidative dehydrogenation process.

The key component for this excellent catalytic behavior seems to be the Ni–Nb solid solution formed upon doping NiO with Nb. Even small amounts of niobium effectively convert NiO from a total oxidation catalyst to a very efficient ODH material. The characterization results show that up to a Nb/Ni atomic ratio of 0.176, Nb^{5+} ions efficiently substitute Ni^{2+} ions and/or fill the cationic vacancies in the NiO lattice, with higher Nb content leading to saturation of the bulk lattices sites and formation of the mixed $NiNb_2O_6$ phase and pure Nb_2O_5. The surface composition of the catalysts, determined by XPS, indicates that the relative exposure of nickel and niobium on the surface is constant irrespective of the nominal Nb/Ni ratio, with the exception of the highest-Nb content catalyst, probably due to the high inhomogeneity and extended segregation of the two phases detected on this sample. To obtain information on the nature of the active sites for ethane activation, the SSAc, expressed as 10^{-2} µmol C_2H_6 consumed/(m^2 s) at 300 °C and differential conditions (conversion < 10%), and the surface concentration of nickel sites are plotted as a function of the nominal Nb/Ni atomic ratio in Fig. 13. A clear correlation between the ability of the catalytic surface to activate the ethane substrate and the number of exposed surface Ni sites is apparent, with these two values following the same trend with increasing Nb/Ni ratio. Based on this observation, we postulate that nickel centers constitute the reactive sites for the activation of alkane, whereas niobium seems to mainly affect the selectivity pattern modifying the route of the reaction from total to selective oxidation to olefin.

What then is the functionality of niobium, and what are the modified properties that lead to the enhanced ODH behavior of the catalysts? XPS, electrical conductivity, and O_2-TPD studies demonstrate that NiO is a highly conductive, nonstoichiometric oxide with cationic vacancies (excess surface oxygen). Based on data in the literature, its conductivity results from the positive holes p^+, which are induced by the cationic vacancies

in the form of Ni^{3+} or O^- ions, to maintain charge neutrality conditions [41,42]. Iwamoto et al. [44] extensively studied the chemisorption of O_2 on NiO and suggested that O_2^- and O^- species are the predominant species formed on the nickel oxide surface. Therefore, nonstoichiometric oxygen desorbed from NiO is believed to be in the form of electrophilic oxygen radicals. The nature and reactivity of the oxygen species on the catalytic surface is believed to be one of the key factors governing the performance of metal oxide catalysts in selective oxidation reactions. It is widely accepted that electrophilic species (O_2^-, O_2^{2-}, O^-) are mostly responsible for the deep oxidation reactions, whereas nucleophilic ones (O^{2-}) are involved in both the selective and unselective steps of the reaction [45].

Consequently, the low selectivity of NiO in the ethane oxidative dehydrogenation reaction and the preferential total oxidation of ethane to CO_2 likely result from the highly reactive electrophilic single-charged oxygen species present on the nickel oxide surface. As the conductivity measurements point out, Nb incorporation causes a one-fold decrease in electrical conductivity, consistent with the principle of controlled valence [25] for dissolution of higher-valence ions in the lattice of p-type host oxide. Niobium, therefore, acts as an electron donor and reduces the positive p^+ hole concentration of the NiO acceptor. In agreement with this finding, the O_2-TPD experiments clearly indicate that Nb consumes or eliminates the incompletely reduced electrophilic oxygen species (e.g., O^-, O_2^-, or O_2^{2-}), thus significantly suppressing the total oxidation of ethane to carbon dioxide and enhancing the selective conversion to ethylene. The excess oxygen accommodated on the surface of Ni-based catalysts reportedly correlates inversely with the selectivity to ethylene [15]. Conclusively, the elimination of nonstoichiometric oxygen caused by Nb doping is very likely responsible for the high ethene selectivity exhibited by the Ni–Nb–O mixed oxides.

5. Conclusion

The present work demonstrates the high potential of a new class of catalytic materials based on nickel as active component for the low-temperature oxidative dehydrogenation of ethane to ethylene. Studying the catalytic performance of a series of Ni–Nb–O mixed oxides (Nb/Ni atomic ratios of 0–0.67) clearly indicates that introducing even small amounts of Nb in NiO converts nickel oxide from an effective total oxidation catalyst to an efficient low-temperature ODH catalyst, producing ethylene with a yield of 46% at 400 °C. An optimum in the catalytic behavior is achieved for the catalyst containing Nb/Ni in an intermediate ratio of 0.176 ($Ni_{0.85}Nb_{0.15}$), which exhibits the highest per weight activity and selectivity to ethylene (90%).

A correlation between the ethane specific surface activity of the catalysts and the surface-exposed nickel content indicates that nickel sites constitute the active centers for activation of the paraffinic substrate, whereas niobium affects mainly the selectivity to the desired product, olefin. NiO is a nonstoichiometric oxide with cationic vacancies, which can accommodate large amounts of excess electrophilic oxygen radicals, strong oxidizing species responsible for the total oxidation of ethane to CO_2 occurring on the NiO surface. Due to the favorable ionic radii of niobium, Nb cations fill the cationic vacancies and/or substitute nickel atoms in the NiO lattice, forming a Ni–Nb solid solution. This substitution process is most likely responsible for the reduction of the nonstoichiometry and the cationic defects on the surface and, consequently, of the unselective oxygen species, leading to enhanced ethane ODH activity.

The effect of niobium on the surface oxygen species participating in the reaction and its enhancing action on the ethylene selectivity is further investigated and confirmed by transient experiments with isotopic $^{18}O_2$, presented in part II of the present series. In addition, aspects of the mechanism and the ethane ODH reaction pathways occurring over this new class of catalytic materials are discussed, and a macroscopic kinetic model able to predict the catalyst performance for a wide range of operating conditions is developed.

Acknowledgments

The authors thank Drs. L. Nalbandian and V. Zaspalis from CERTH/CPERI for providing the facilities for XRD, SEM, and conductivity measurements and Drs. A.F. Lee and K. Wilson of York University for helping with the XPS measurements. Financial support was provided by the General Secretariat of Research and Technology Hellas (grant PENED01).

References

[1] G. Centi, F. Cavani, F. Trifiro, Selective Oxidation by Heterogeneous Catalysis, Kluwer Academic Publishers/Plenum Press, New York, 2001.
[2] M.A. Banares, Catal. Today 5 (1999) 319.
[3] H.X. Dai, C.T. Au, Curr. Top. Catal. 3 (2002) 33.
[4] H.H. Kung, Adv. Catal. 40 (1994) 1.
[5] E. Heracleous, A.F. Lee, I.A. Vasalos, A.A. Lemonidou, Catal. Lett. 88 (2003) 47.
[6] E. Heracleous, M. Machli, A.A. Lemonidou, I.A. Vasalos, J. Mol. Catal. A 232 (2005) 29.
[7] S.J. Conway, J.H. Lunsford, J. Catal. 131 (1991) 513.
[8] E. Morales, J.H. Lunsford, J. Catal. 118 (1989) 255.
[9] L. Leveles, S. Fuchs, K. Seshan, J.A. Lercher, L. Lefferts, Appl. Catal. A 227 (2002) 287.
[10] S. Gaab, M. Machli, J. Find, R.K. Grasselli, J.A. Lercher, Top. Catal. 23 (2003) 151.
[11] E.M. Thorsteinson, T.P. Wilson, F.G. Young, P.H. Kasai, J. Catal. 52 (1978) 116.
[12] P. Botella, E. Garcia-Gonzalez, A. Dejoz, J.M. Lopez Nieto, M.I. Vazquez, J. Gonzalez-Calbet, J. Catal. 225 (2004) 428.
[13] E. Heracleous, A.F. Lee, K. Wilson, A.A. Lemonidou, J. Catal. 231 (2005) 159.
[14] Y. Schuurman, V. Ducarme, T. Chen, W. Li, C. Mirodatos, G.A. Martin, Appl. Catal. A 163 (1997) 227.
[15] X. Zhang, Y. Gong, G. Yu, Y. Xie, J. Mol. Catal. A 180 (2002) 293.
[16] X. Zhang, J. Liu, Y. Jing, Y. Xie, Appl. Catal. A 240 (2003) 143.
[17] Y. Liu, US Patent 6 436 871 (2002), to Symyx Technologies.
[18] Y. Liu, US Patent 6 417 422 (2002), to Symyx Technologies.
[19] A.K. Jonscher, Nature 267 (1977) 673.
[20] S. Lee, H.M. Cheong, N. Park, C.E. Tracy, A. Mascarenhas, D.K. Benson, S.K. Deb, Solid State Ionics 140 (2001) 135.
[21] A. Ponchel, A. D'Huysser, C. Lamonier, L. Jalowiecki-Duhamel, Phys. Chem. Chem. Phys. 2 (2000) 303.
[22] A.C. Faro, P. Grange, A.C.B. dos Santos, Phys. Chem. Chem. Phys. 4 (2002) 3997.
[23] J. Jehng, I.E. Wachs, Catal. Today 8 (1990) 37.

[24] K. Tanabe, in: M. Boudart, J.R. Anderson (Eds.), Catalysis Science and Technology, vol. 2, Springer, Berlin, 1983.
[25] P.A. Cox, Transition Metal Oxides: An Introduction to Their Electronic Structure and Properties, Oxford Univ. Inc., New York, 1992, pp. 170–178.
[26] I. Nowak, M. Ziolek, Chem. Rev. 99 (1999) 3603.
[27] J.M. Jehng, I.E. Wachs, Chem. Mater. 3 (1991) 100.
[28] L.J. Burcham, J. Datka, I.E. Wachs, J. Phys. Chem. B 103 (1999) 6015.
[29] J.M. Herrmann, in: B. Imelik, J.C. Védrine (Eds.), Catalyst Characterization Physical Techniques for Solid Materials, Plenum Press, New York, 1994, p. 559.
[30] G.H. Yi, T. Hayakawa, A.G. Andersen, K. Suzuki, S. Hamakawa, A.P.E. York, M. Shimizu, K. Takehira, Catal. Lett. 38 (1996) 189.
[31] Q.J. Ge, B. Zhaorigetu, C.Y. Yu, W.Z. Li, H.Y. Xu, Catal. Lett. 68 (2000) 59.
[32] B. Zhaorigetu, W. Li, H. Xu, R. Kieffer, Catal. Lett. 94 (2004) 125.
[33] P. Viparelli, P. Ciambelli, J.C. Volta, J.M. Herrmann, Appl. Catal. A 182 (1999) 165.
[34] E.V. Kondratenko, M. Baerns, Appl. Catal. A 222 (2001) 133.
[35] I.C. Marcu, J.M.M. Millet, J.M. Herrmann, Catal. Lett. 78 (2002) 273.
[36] L.M. Madeira, J.M. Herrmann, F.G. Freire, M.F. Portela, F.J. Maldonado, Appl. Catal. A 158 (1997) 243.
[37] A.M.D. Farias, W. Gonzalez, P.G. Pries, J.G. Eon, J.M. Herrmann, M. Aouine, S. Loridant, J.C. Volta, J. Catal. 208 (2002) 238.
[38] A.M. Turky, Appl. Catal. A 247 (2003) 83.
[39] A. Bielanski, R. Dzeinbaj, J. Slozynski, Bull. Acad. Pol. Sci. 14 (1966) 569.
[40] M.E. Dry, F. Stone, Discuss. Faraday Soc. 58 (1959) 192.
[41] M. Atanasov, D. Reinen, J. Electron. Spectrosc. Relat. Phenom. 86 (1997) 185.
[42] E. Antolini, Mater. Chem. Phys. 82 (2003) 937.
[43] T. Chen, W. Li, C. Yu, R. Jin, H. Xu, Stud. Surf. Sci. Catal. 130 (2000) 1847.
[44] M. Iwamoto, Y. Yoda, M. Egashira, T. Seiyama, J. Phys. Chem. 80 (1976) 1989.
[45] A. Bielanski, J. Haber, Oxygen in Catalysis, Dekker, New York, 1991.